Effect of particle size on the biodistribution of lipid nanocapsules: Comparison between nuclear and fluorescence imaging and counting.

Samuli Hirsjärvi, Lucie Sancey, Sandrine Dufort, Camille Belloche, Claire Vanpouille-Box, Emmanuel Garcion, Jean-Luc Coll, François Hindré, Jean-Pierre Benoit

Effect of particle size on the biodistribution of lipid nanocapsules: comparison between nuclear and fluorescence imaging and counting

Samuli Hirsjärvi[a,1,*], Lucie Sancey[b,c,1], Sandrine Dufort[b], Camille Belloche[a], Claire Vanpouille-Box[a,d], Emmanuel Garcion[a], Jean-Luc Coll[b], François Hindré[a], Jean-Pierre Benoît[a]

[a] LUNAM Université, Université d'Angers, INSERM U1066, Angers, France

[b] INSERM-UJF-CRI-U823, Institut Albert Bonniot, La Tronche, France

[c] UMR 5306 CNRS – Université Claude Bernard Lyon 1, Laboratoire de Physico-Chimie des Matériaux Luminescents, Villeurbanne, France

[d] Present affiliation: New York University School of Medicine, Department of Pathology, New York, NY, USA

[1] Equal contribution

[*] *Corresponding author* (S. Hirsjärvi): samuli.hirsjarvi@univ-angers.fr, tel.: +33 2 44 68 85 45; fax: +33 2 44 68 85 46; address: INSERM U1066, IBS-CHU Angers, 4 rue Larrey, 49933 Angers, France.

Abstract

In vivo biodistribution of nanoparticles depends on several physicochemical parameters such as size. After intravenous injection of 25, 50 and 100 nm lipid nanocapsules (LNC) in *nude* mice bearing HEK293(β_3) tumour xenografts, biodistribution was evaluated by γ-scintigraphy and by γ-counting. The small LNC 25 nm disappeared faster than the larger LNC 50 and 100 nm from the blood circulation due to faster elimination and wider tissue distribution. At 24 h, biodistribution profiles of all these LNC were similar. Low LNC quantities were found in this weak EPR (enhanced permeability and retention) tumour regardless the particle size. Co-injected 50 nm fluorescent DiD-LNC and ^{99m}Tc-LNC allowed direct comparison of biodistribution as evaluated by the two methods. Optical imaging underestimated LNC quantity especially in dark-coloured organs that were observed to capture extensive quantities of the particles by γ-counting (*i.e.* liver, spleen, and kidney).

Keywords: lipid nanocapsules, biodistribution, γ-scintigraphy, optical imaging, fluorescence

1 Introduction

Extensive studying of nanoparticles during the last decades has resulted in drug delivery systems that protect the active substance, improve solubility and carry the drug to specific tissues in the body (Farokhzad and Langer, 2009). Cancer therapy is one of the areas that benefit considerably from these advances (Hirsjärvi et al., 2011). In order to develop an efficient nanoparticulate drug delivery system, its pharmacokinetic profile as well as biodistribution should be evaluated when the system is transferred from *in vitro* assays to first preclinical tests. Molecular imaging offers tools for non-invasive evaluation (Baker, 2010), and the same probes used also allow tissue distribution determination after animal sacrifice. Commonly used small animal imaging technologies include X-ray computed tomography (CT), magnetic resonance imaging (MRI), positron emission tomography (PET), single photon emission computed tomography (SPECT) and different optical imaging techniques (Dufort et al., 2010). Optical imaging techniques are sensitive, non-ionizing, fast and easy to perform, portative and cheap. However, quantitative performance of optical techniques still needs improvement in order to overcome the problems of absorption and autofluorescence. SPECT can overcome optical imaging problems because it provides more reliable quantitative information about physiological functions at the molecular level and it is, thus, well suited for monitoring many vital processes such as blood flow and perfusion, receptor-ligand binding rates, and oxygen utilization. SPECT has no depth limit but the acquisition times might be from several minutes up to hours. However, SPECT suffers from some noteworthy other disadvantages such as the need of radiolabelled particles, and adapted and expensive devices. Both SPECT and optical imaging possess a resolution of 1 mm (for more detail, please see (Dufort et al., 2010)).

Biocompatible nanoparticles for drug delivery are usually made of polymer or lipid materials (Kumari et al., 2010; Müller et al., 2011; Torchilin, 2007; Torchilin, 2005). Lipid nanocapsules

(LNC) are synthetic particles having a hybrid structure between polymer nanoparticles and liposomes (Heurtault et al., 2002). LNC consist of low-toxicity materials (PEGylated surfactant, lecithin, triglycerides) and their fabrication, based on low-energy organic solvent-free phase inversion process, can be easily scaled up. By changing proportions of the components, the LNC size can be tuned within the range of 20-100 nm (Heurtault et al., 2003). LNC have been applied *e.g.* in the delivery of cancer therapeutics (Cirpanli et al., 2011; Garcion et al., 2006; Lacoeuille et al., 2007; Paillard et al., 2010; Peltier et al., 2006; Weyland et al., 2011) and other drug molecules (Lamprecht et al., 2004) as well as macromolecules such as siRNA and DNA (Morille et al., 2010; Morille et al., 2011). Because of their semi-rigid shell, LNC can be modified by post-inserting amphiphilic molecules. This kind of post-insertion allows for *e.g.* improvement of biodistribution profiles (Hoarau et al., 2004; Morille et al., 2010) or creation of templates for further attachment of active targeting ligands (Béduneau et al., 2008; Béduneau et al., 2007; Bourseau-Guilmain et al., 2012). Radioactive molecules such as ^{99m}Tc and ^{188}Re have been successfully encapsulated in LNC as forms of lipophilic complexes (Ballot et al., 2006). These kinds of radio-labelled LNC can be used in biodistribution studies, imaging purposes and in radiotherapy (Allard et al., 2008; Ballot et al., 2006; Vanpouille-Box et al., 2011a; Vanpouille-Box et al., 2011b).

In a previous study, we have evaluated the biodistribution profile of LNC of three different sizes (25, 50 and 100 nm) with the help of an optical imaging technique, fluorescence reflectance imaging (2D-FRI) (Hirsjärvi et al., 2013). *Nude* mice bearing subcutaneous HEK293(β_3) (human embryonic kidney) xenografts were used in the study. Images taken at 1.5-3 h after intravenous injection revealed that fluorescence staining of the smallest LNC (25 nm) was more homogeneous throughout the mice than the staining of the bigger LNC: the 50 and 100 nm LNC were found mostly in the liver. However, when the mice were sacrificed after 24 h, tissue distribution profiles,

evaluated by fluorescence intensity, were similar for the three LNC sizes. With all three sizes, tumour could be distinguished from the images.

In the present study, to get more quantitative information about LNC pharmacokinetics and biodistribution, ^{99m}Tc-labelled LNC of the same three sizes (25, 50 and 100 nm) were injected intravenously in *nude* mice bearing the same tumour model (HEK293(β_3) xenografts). γ-Scintigraphy was performed at different time points up to 24 h together with tissue distribution determination by γ-counting at 1.5, 4 and 24 h. To compare the performance of 2D-FRI imaging (region of interest (ROI) drawing around each organ from the images taken with a fluorescence camera) and γ-counting in the determination of tissue distribution, mice were co-injected a mixture of fluorescence-labelled (DiD) and ^{99m}Tc-labelled LNC of one chosen size (50 nm).

2 Materials and Methods

2.1 Materials

Solutol® HS15 (PEG 660 12-hydroxystearate, M_W ~ 870 Da) (BASF, Ludwigshafen, Germany), Labrafac™ WL 1349 (caprylic/capric acid triglycerides) (Gattefossé S.A., Saint-Priest, France), Lipoid® S75-3 (M_W ~ 780 Da) (Lipoid GmbH, Ludwigshafen, Germany), NaCl (Prolabo VWR International, Fontenay-sous-Bois, France) and deionized MilliQ185 water (Waters, Saint-Quentin-en-Yveline, France) were used in the LNC preparation. 1,1'-dioctadecyl-3,3,3',3'-tetramethylindodicarbocyanine perchlorate (DiD) was from Invitrogen (Cergy Pontoise, France).

2.2 Methods

2.2.1 Preparation of the ^{99m}Tc-SSS complex

Pertechnetate ($^{99m}TcO_4^-$) was obtained from the University Hospital of Angers (CHU Angers, France). The ^{99m}Tc-SSS complex (bis (perthiobenzoato) (dithiobenzoato) technetium(III) heterocomplex) was prepared according to the following method (Ballot et al., 2006; Mévellec et al., 2002): 750 MBq of $^{99m}TcO_4^-$ in 0.5 mL 0.9% NaCl was added to a freeze-dried formulation kit containing 30 mg sodium gluconate, 30 mg ascorbic acid, 40 mg potassium oxalate, and 4 mg $SnCl_2 \cdot 2H_2O$ reconstituted in 0.5 mL 0.9% NaCl, and the solution was mixed for 15 minutes at room temperature. Then, 20 mg of sodium dithiobenzoate ligand (in 0.5 mL, pH 7) (Platform of Organic Synthesis, Rennes, France) was added and the mixture was heated at 100 °C for 30 minutes, which allowed formation of the ^{99m}Tc-SSS complex. The complex was extracted with dichloromethane (1 mL) and washed three times with 1 mL water.

2.2.2 LNC preparation and characterization

LNC were prepared by the phase inversion temperature method described by Heurtault *et al.* (Heurtault et al., 2003). Solutol®, Lipoid®, Labrafac®, NaCl and water were mixed and the ^{99m}Tc-SSS complex in dichloromethane (^{99m}Tc-LNC) or DiD in acetone (DiD-LNC) was added to this mixture. When preparing fluorescent LNC, final concentration of DiD was 3 mmol/L / total Labrafac® amount. Dichloromethane/acetone was evaporated by heating at 60 °C for 15 min under stirring. The formulation was heated to 85 °C at a rate of 5 °C / min followed by cooling at the same rate to 65 °C. This cycle was repeated twice. During the last decrease of temperature, at 78 °C (during the phase inversion zone), the system was diluted with 4.2 mL cold (4 °C) water leading to

formation of stable LNC. Size of the LNC (25, 50, 100 nm) was adjusted by changing the proportions of the components (Table 1).

Size distributions and zeta (ζ) potentials of LNC were determined with a Zetasizer ZS (Malvern, Worcestershire, UK). Particle sizing was based on photon correlation spectroscopy (PCS); the results were analyzed by CONTIN algorithm and the sizes were presented based on the volume distributions together with polydispersity indices (PdI). Electrophoretic mobilities were converted to ζ-potentials using Smoluchowski's equation.

2.2.3 Cells

HEK293(β_3) cells, stable transfectants of human β_3 from the human embryonic kidney cell line (kindly provided by J.-F. Gourvest, Aventis, France), were cultured in DMEM supplemented with 1% glutamine, 10% fetal bovine serum (FBS), 50 units/mL penicillin, 50 µg/mL streptomycin, and 700 µg/mL Geneticin (G418 sulfate, Gibco, Paisley, UK), at 37 °C in a humidified 95% air / 5% CO_2 atmosphere.

2.2.4 In vivo imaging and biodistribution study

The animal experiments were performed in agreement with the EU Directive 2010/63/EU for animal experiments, and the "Principles of Laboratory Animal Care" (NIH Publication no. 86-23, revised 1985), and the experimental protocol was approved by the local ethics committee.

40 female NMRI *nude* mice (5 weeks old, JANVIER, Le Genest Saint Isle, France) were injected subcutaneously with HEK293(β_3) cells (1×10^7 / mouse). After tumor growth (~ 4 weeks), mice

were anesthetized with a mixture of ketamine (100 µg/g) / medetomidine (0.2 µg/g) by an intraperitoneal injection, and then 200 µL of LNC (about 100 mg/mL) were injected intravenously in the tail vein. Thus, each mouse obtained a dose of about 26 MBq ^{99m}Tc (^{99m}Tc-LNC). The mice which were injected by the mixture radio- and fluorescence-labelled LNC obtained 100 µL of ^{99m}Tc-LNC (13 MBq) and 100 µL of DiD-LNC (same quantity of both LNC).

In γ-scintigraphy, the injected mice were visualized under a clinical γ-camera (Sopha Medical DSXi, 140 keV±15%, 128^2 matrix, HRLE collimator). Static 15 min scintigraphic images were registered at 1.5 h, 3 h, 5h, and 24 h (a video clip of dynamic 30 s scintigraphic acquisitions collected until 90 min post-injection is available as Supporting Content). To study tissue distribution of LNC, the animals were sacrificed at 1.5 h (n = 4), 4 h (n = 4), and 24 h (n = 4) after injection. The organs/tissues were removed, rinsed, and weighed. Activity of each removed organ was determined using a γ-counter (Packard Auto-Gamma 5,000 series).

Fluorescent images were acquired by a back-thinned CCD camera at -80°C (ORCAII-BT-512G, Hamamatsu, Massy, France). Image display and analysis of the dissected organs were performed using the Wasabi software (Hamamastsu, Massy, France). Semi-quantitative data were obtained by drawing regions of interest (ROI) around each organ. The results of organ fluorescence quantifications were expressed as number of relative light units (RLU)/pixel.

When imaging and quantifying the mice that obtained the mixture of radio- and fluorescence-labelled LNC, fluorescence acquisitions were performed before scintigraphic acquisitions and γ-counting.

2.2.5 Statistical analysis

Biodistribution data was analyzed using one-way ANOVA with Tukey's multiple comparison test (Prism, GraphPad Software, Inc., La Jolla, CA). $p < 0.05$ was considered as statistically significant.

3 Results

3.1 LNC preparation

Size and ζ-potential of ^{99m}Tc-LNC are presented in Table 2. These characteristics of DiD-LNCs were identical with ^{99m}Tc-LNC (Hirsjärvi et al., 2013). PdI-values of all three types of LNC were low indicating homogeneous size distributions. Slightly negative ζ-potential of LNC originates from PEG groups at the surface forming dipoles able to interact with counterions or water dipoles (Vonarbourg et al., 2005). Encapsulation of lipophilic ^{99m}Tc or DiD in the oily core of LNC did change neither size nor ζ-potential of the blank LNC as reported earlier (Ballot et al., 2006; Morille et al., 2010; Paillard et al., 2010; Zou et al., 2008).

3.2 In vivo biodistribution of ^{99m}Tc-LNC

Biodistribution of 25, 50, and 100 nm ^{99m}Tc-LNC in different organs 1.5 h, 4 h and 24 h after i.v. injections are presented in Figure 1. LNC 25 nm disappeared quickly from the blood circulation: 3-6% total CPM (counts per minute) / g of the 25 nm LNC was found in the blood at 1.5-4 h whereas the measured blood activities for LNC 50/100 nm were about 25-30 % at the same time points ($p < 0.001$: LNC 25 nm *vs.* LNC 50/100 nm). Conversely, at 24 h, total CPM / g of LNC 25 nm was higher (~3%) than the corresponding LNC 50/100 nm values (~1.5%; $p < 0.01$). More activity of

LNC 25 nm was found in the liver at 1.5-4 h (~28%) compared to LNC 50 nm (16-18%; $p < 0.01$) and LNC 100 nm (21-22%; difference not significant). Also, compared to LNC 50/100 nm, more LNC 25 nm were found in the heart and in the lung ($p < 0.01$), and in the adrenal at 1.5-4 h. In contrast, at 24 h, less LNC 50 nm was found in the heart, lung and kidney compared to LNC 25/100 nm ($p < 0.05$). The spleen captured less LNC 50 nm than LNC 25/100 nm at 1.5 h and 4 h ($p < 0.05$). No significant differences were found in the tumour accumulation between the three particle sizes at different time points (1-3% total CPM / g). Otherwise, distribution in other organs was similar at different time points.

γ-Scintigraphic images of mice 1.5 h, 3 h, 5 h, and 24 h after i.v. injection of 25, 50 and 100 nm ^{99m}Tc-LNC are presented in Figure 2. The livers were well visible at 24 h. At earlier time points, especially at 1.5 h and 3 h, more vertical highlighted regions revealed also radioactivity in the blood circulation (heart, lungs). LNC 25 nm were better observable than LNC 50/100 nm in peripheral regions and at intestinal area of mice at 3 h and 5 h. These observations were supported by the γ-counting results: if the values "% CPM of all organs" were not corrected by the organ masses, radioactivity in the carcass after the injection of LNC 25 nm were 39% at 1.5 h and 37% at 4 h. Corresponding values for LNC 50 and 100 nm were 22% ($p < 0.001$ *vs.* LNC 25 nm) and 22% ($p < 0.001$); 15% ($p < 0.01$) and 18% ($p < 0.05$) at 1.5 h and 4 h, respectively. Also, at 4 h, 7.5% of LNC 25 nm were found in the intestine *vs.* 4.5% of LNC 50 nm and 3% of LNC 100 nm (both $p < 0.01$ *vs.* LNC 25 nm).

3.3 Comparison of in vivo biodistribution of co-injected ^{99m}Tc-LNC and DiD-LNC

An example of fluorescence images of a mouse 24 h after injection of a 50%-50% mixture of 50 nm DiD-LNC and ^{99m}Tc-LNC is presented in Figure 3. Fluorescence staining allowed identifying of the

liver (A) and the tumour (B). LNC biodistribution in different organs at 24 h is presented in Figure 4. To better compare the quantification by the two techniques (γ-counting and fluorescence imaging), the organ data were normalized by the detected radioactivity (% ID/g) and fluorescence intensity (RLU/pixel/20 ms) in the bone. As already observed when testing radiolabelled LNC of different sizes, the majority of radioactivity was found in the liver as well as in the adrenal, spleen, and kidneys (Fig. 4A). Instead, the observed fluorescence intensity was also highest in the liver, but the next highest fluorescent organs were the ovaries, adrenal, and skin. The global fluorescence intensity in the spleen was low, and moderate in the kidneys. Radioactivity in relation to other organs was clearly higher in the liver, adrenal, spleen, kidney, ovary, and lung. No such clear differences were observed in fluorescence intensities. An image of the organs (Fig. 4B), used for the quantification, reveals well the highly fluorescent organs.

4 Discussion

Generally, sub-100 nm nanoparticles are expected to circulate longer time in the blood compared to > 100 nm particles (Vonarbourg et al., 2006). However, in the size range of 10-100 nm, surface and even elasticity properties of nanoparticles as well as their mechanism of elimination have been shown to dictate pharmacokinetic and biodistribution profiles. Also, animal model (mouse/rat) is known to affect tissue distribution (Sun et al., 2005). For example, systemic clearance and volume of distribution of 60 nm PEGylated polyacrylate nanoparticles in mice were significantly lower when compared to 20 nm particles, leading to lower liver uptake (~15% ID/g at 48 h) of the larger 60 nm particles (Yang et al., 2009). Similarly, 25 nm polymer micelles exhibited much shorter circulation half-lives than 60 nm micelles (2.2-fold decrease in the distribution phase $t_{1/2}$) (Lee et al., 2010). More efficient clearance by hepatobiliary excretion of the smaller micelles was proposed as ~70% of the (mouse) liver fenestrations are narrower than 100 nm. The longest blood half-life of

10-100 nm PEGylated gold nanoparticles was achieved with ~60 nm particles by adjusting the size and PEG length (Perrault et al., 2009). On the other hand, mice plasma clearance rates (12% ID/mL plasma at 24 h), and the quantities in kidney (~4% ID/g), liver (10-16% ID/g) and in spleen (5-10% ID/g) were similar regardless of the polymer micelle size (30-100 nm) (Cabral et al., 2011). Several studies have proposed wider distribution, extravasation, of nanoparticles in different organs, the smaller the particle size was in the sub-100 nm range (De Jong et al., 2008; Hirn et al., 2011; Sonavane et al., 2008; Yang et al., 2009). Similarly to our results with 25, 50, and 100 nm LNC, shortened blood circulation time is frequently related to this wider biodistribution. Higher quantity of LNC 25 nm in the liver (1.5, 4 h) compared to LNC 50/100 nm in the current study indicated also faster hepatic accumulation. Radioactivity found in the kidneys can be explained by LNC accumulation. To undergo a complete renal clearance, the nanoparticle size should be less than 10 nm (Choi et al., 2007). Instead, 75±25 nm PEGylated gold nanoparticles are reported to enter the fenestrated glomerular endothelia (80-100 nm pores) and accumulate in the kidney mesangium (Choi et al., 2011). Nanoparticle accumulation in the ovaries, clearly visible in the case of LNC (Fig. 4), is assumed to originate from fast growing and, thus, highly vascularized nature of the ovarian corpus luteum of mature female mice that leads to the EPR (enhanced permeability and retention) effect, described initially for tumours (Schädlich et al., 2012).

In our previous study, after i.v. injection, signals of fluorescent-labelled LNC 25 nm in the skin and in the intestine were found to be more intense than the corresponding signals of LNC 50/100 nm (Hirsjärvi et al., 2013). Thus, the results of the current study confirmed these findings. Almost twice the radioactivity of LNC 25 nm in carcass compared to LNC 50/100 nm at 1.5-4 h indicated, indeed, that the smallest LNC were distributed rapidly to the peripheral capillaries and probably perfused further to tissues increasing the skin fluorescence. Higher LNC 25 nm quantities in the intestine suggested more pronounced hepato-biliary evacuation. Differences in the elimination rate

of the three LNC could not be, however, revealed when estimated injected doses were compared to CPM of all organs. For each LNC type, differences between the different time points remained within 10% and were not significantly different.

Magnitude of the tumour accumulation of nanoparticles by the EPR effect together with a therapeutic effect (of an encapsulated drug) remains in general in the range of 3.5-12% (ID/g) (de Wolf et al., 2007; Kircheis et al., 2002; Kursa et al., 2002; Meng et al., 2011). Accumulation of LNC 25-100 nm in HEK293(β_3) tumour was a bit lower (1-3%). It should be noted, however, that this subcutaneous model is an "EPR-weak" tumour having well-structured, neo-angiogenic vasculature with tight endothelial junctions (Jin et al., 2007; Razkin et al., 2006).

γ-Imaging of dual-labelled (radio+fluorescence) PEGylated polyacrylate nanoparticles revealed radioactivity in the cardiac area at early observation time points (5 min – 4 h) followed by increasing activity in liver and spleen up to 48 h (Yang et al., 2009). Tumour was poorly observable by γ-imaging but, instead, optical imaging that enhanced subcutaneous signal compared to deep signals, showed clear fluorescence staining in tumour. Subcutaneous tumours were well visualized by strongly surface-weighted optical imaging. Therefore, as in our studies ((Hirsjärvi et al., 2013) and the current study), optical imaging offers better resolution imaging especially for superficial organs whereas γ-scintigraphy recapitulates the global biodistribution of radiolabelled compounds in both internal and superficial organs.

To better compare the biodistribution of LNC measured by the two techniques, radioactivity and fluorescence intensity, the corresponding results were normalized by the value observed in the bone. The bone was selected because its radioactivity / fluorescence intensity level was observed to be settled in the middle of all analysed organs, allowing, thus, distinct representation of the data. In

order to quantify fluorescence intensity of dissected organs, graphical ROI estimation from images visualized by a fluorescent camera is commonly performed. (Goutayer et al., 2010; Kim et al., 2010; Na et al., 2011; Sancey et al., 2009; Schädlich et al., 2011a; Schädlich et al., 2011b; Yang et al., 2007). Alternatively, homogenization of each dissected organ followed by determination of the fluorescence intensity on a microtiter plate can be done (He et al., 2010; Meng et al., 2011). The fluorescence intensity technique (ROI drawing and estimation), compared to γ-counting, underestimated the LNC proportion in all the red and the dark red organs such as RES organs (liver, lung, spleen), and the kidney and adrenal. These organs are characterized by high blood perfusion. Similarly to our findings, *ex vivo* quantification of fluorescence intensity underestimated the uptake of polymer micelles in the liver, spleen, kidney, and also in the heart (Yang et al., 2007). For this reason, relative fluorescence intensity in other organs was found to be emphasized. Because of the fluorescence quantification technique in this study, intensities of thin organs (*i.e.* skin) were also slightly highlighted. It should be noted that direct comparison of the two quantification techniques after normalization (Fig. 4) is not recommendable but, instead, this approach revealed well the relative differences between the organs within each technique.

5 Conclusions

Biodistribution studies of radiolabelled ^{99m}Tc-LNC in *nude* mice with subcutaneous HEK293(β_3) xenografts revealed that the majority of the smallest studied particles (25 nm) disappeared quickly from the blood circulation within 1.5 h after the intravenous injection due to wider tissue distribution and faster elimination. Instead, 50 and 100 nm LNC remained in the circulation at least up to 4 h. At 24 h, biodistribution profiles of the all LNC were similar. Tumour accumulation of LNC in this EPR-weak tumour was low regardless the size. When biodistribution profiles of co-injected 50 nm fluorescent DiD-LNC and ^{99m}Tc-LNC after animal sacrifice were compared,

underestimating tendency of fluorescence detection of LNC accumulation in highly-capturing and perfused organs (liver, adrenal, spleen, kidney, lung) was clearly observed but fluorescence detection allowed visualization of the tumour area. In following studies, we will further concentrate on the comparison of the two imaging / biodistribution evaluation techniques with the help of dual-labelled nanocarriers and different tumour models.

Acknowledgements

This work was financially supported by the French National Research Agency (ANR) in the frame of its programme in Nanosciences and Nanotechnologies (CALIF project no. ANR-08-NANO-006).

References

Allard, E., Hindre, F., Passirani, C., Lemaire, L., Lepareur, N., Noiret, N., Menei, P., Benoit, J.P., 2008. Re-188-loaded lipid nanocapsules as a promising radiopharmaceutical carrier for internal radiotherapy of malignant gliomas. Eur J Nucl Med Mol Imag 35, 1838-1846.

Baker, M., 2010. Whole-animal imaging: the whole picture. Nature 463, 977-980.

Ballot, S., Noiret, N., Hindré, F., Denizot, B., Garin, E., Rajerison, H., Benoit, J.-P., 2006. ^{99m}Tc/^{188}Re-labelled lipid nanocapsules as promising radiotracers for imaging and therapy: Formulation and biodistribution. Eur J Nucl Med Mol Imag 33, 602-607.

Béduneau, A., Hindré, F., Clavreul, A., Leroux, J.-C., Saulnier, P., Benoit, J.-P., 2008. Brain targeting using novel lipid nanovectors. J Control Release 126, 44-49.

Béduneau, A., Saulnier, P., Hindré, F., Clavreul, A., Leroux, J.-C., Benoit, J.-P., 2007. Design of targeted lipid nanocapsules by conjugation of whole antibodies and antibody Fab' fragments. Biomaterials 28, 4978-4990.

Bourseau-Guilmain, E., Béjaud, J., Griveau, A., Lautram, N., Hindré, F., Weyland, M., Benoit, J.P., Garcion, E., 2012. Development and characterization of immuno-nanocarriers targeting the cancer stem cell marker AC133. Int J Pharm 423, 93-101.

Cabral, H., Matsumoto, Y., Mizuno, K., Chen, Q., Murakami, M., Kimura, M., Terada, Y., Kano, M.R., Miyazono, K., Uesaka, M., Nishiyama, N., Kataoka, K., 2011. Accumulation of sub-100 nm polymeric micelles in poorly permeable tumours depends on size. Nature Nanotechnol 6, 815-823.

Choi, C.H.J., Zuckerman, J.E., Webster, P., Davis, M.E., 2011. Targeting kidney mesangium by nanoparticles of defined size. PNAS 108, 6656-6661.

Choi, H.S., Wenhao, L., Misra, P., Tanaka, E., Zimmer, J.P., Ipe, B.I., Bawendi, M.G., Frangioni, J.V., 2007. Renal clearance of quantum dots. Nat Biotech 25, 1165-1170.

Cirpanli, Y., Allard, E., Passirani, C., Bilensoy, E., Lemaire, L., Calis, S., Benoit, J.-P., 2011. Antitumoral activity of camptothecin-loaded nanoparticles in 9L rat glioma model. Int J Pharm 403, 201-206.

De Jong, W.H., Hagens, W.I., Krystek, P., Burger, M.C., Sips, A.J.A.M., Geertsma, R.E., 2008. Particle size-dependent organ distribution of gold nanoparticles after intravenous administration. Biomaterials 29, 1912-1919.

de Wolf, H.K., Snel, C.J., Verbaan, F.J., Schiffelers, R.M., Hennink, W.E., Storm, G., 2007. Effect of cationic carriers on the pharmacokinetics and tumor localization of nucleic acids after intravenous administration. Int J Pharm 331, 167-175.

Dufort, S., Sancey, L., Wenk, C., Josserand, V., Coll, J.L., 2010. Optical small animal imaging in the drug discovery process. Biochim Biophys Acta 1798, 2266-2273.

Farokhzad, O.C., Langer, R., 2009. Impact of nanotechnology on drug delivery. ACS Nano 3, 16-20.

Garcion, E., Lamprecht, A., Heurtault, B., Paillard, A., Aubert-Pouessel, A., Denizot, B., Menei, P., Benoit, J.P., 2006. A new generation of anticancer, drug-loaded, colloidal vectors reverses multidrug resistance in glioma and reduces tumor progression in rats. Mol Cancer Ther 5, 1710-1722.

Goutayer, M., Dufort, S., Josserand, V., Royère, A., Heinrich, E., Vinet, F., Bibette, J., Coll, J.-L., Texier, I., 2010. Tumor targeting of functionalized lipid nanoparticles: Assessment by in vivo fluorescence imaging. Eur J Pharm Biopharm 75, 137-147.

He, C., Hu, Y., Yin, L., Tang, C., Yin, C., 2010. Effects of particle size and surface charge on cellular uptake and biodistribution of polymeric nanoparticles. Biomaterials 31, 3657-3666.

Heurtault, B., Saulnier, P., Pech, B., Proust, J.-E., Benoit, J.-P., 2002. A novel phase inversion-based process for the preparation of lipid nanocarriers. Pharm Res 19, 875-880.

Heurtault, B., Saulnier, P., Pech, B., Venier-Julienne, M.-C., Proust, J.-E., Phan-Tan-Luu, R., Benoit, J.-P., 2003. The influence of lipid nanocapsule composition on their size distribution. Eur J Pharm Sci 18, 55-61.

Hirn, S., Semmler-Behnke, M., Schleh, C., Wenk, A., Lipka, J., Schäffler, M., Takenaka, S., Möller, W., Schmid, G., Simon, U., Kreyling, W.G., 2011. Particle size-dependent and surface charge-dependent biodistribution of gold nanoparticles after intravenous administration. Eur J Pharm Biopharm 77, 407-416.

Hirsjärvi, S., Dufort, S., Gravier, J., Texier, I., Qiao, Y., Bibette, J., Sancey, L., Josserand, V., Passirani, C., Benoit, J.-P., Coll, J.-L., 2013. Influence of size, surface coating and fine chemical composition on the *in vitro* reactivity and *in vivo* biodistribution of lipid nanocapsules *versus* lipid nanoemulsions in cancer models. Nanomedicine: NBM 9, 375-387.

Hirsjärvi, S., Passirani, C., Benoit, J.-P., 2011. Passive and active tumour targeting with nanocarriers. Curr Drug Discov Technol 8, 188-196.

Hoarau, D., Delmas, P., David, S., Roux, E., Leroux, J.-C., 2004. Novel long-circulating lipid nanocapsules. Pharm Res 21, 1783-1789.

Jin, Z.-H., Josserand, V., Foillard, S., Boturyn, D., Dumy, P., Favrot, M.-C., Coll, J.-L., 2007. *In vivo* optical imaging of integrin α_v-β_3 in mice using multivalent or monovalent cRGD targeting vectors. Mol Cancer 6, 41.

Kim, J.-Y., Choi, W.I., Kim, Y.H., Tae, G., Lee, S.-Y., Kim, K., Kwon, I.C., 2010. *In-vivo* tumor targeting of pluronic-based nano-carriers. J Control Release 147, 109-117.

Kircheis, R., Ostermann, E., Wolschek, M.F., Lichtenberger, C., Magin-Lachmann, C., Wightman, L., Kursa, M., Wagner, E., 2002. Tumor-targeted gene delivery of tumor necrosis factor-α induces tumor necrosis and tumor regression without systemic toxicity. Cancer Gene Ther 9, 673-680.

Kumari, A., Yadav, S.K., Yadav, S.C., 2010. Biodegradable polymeric nanoparticles based drug delivery systems. Colloid Surf B 75, 1-18.

Kursa, M., Walker, G.F., Roessler, V., Ogris, M., Roedl, W., Kircheis, R., Wagner, E., 2002. Novel shielded transferrin-polyethylene glycol-polyethylenimine/DNA complexes for systemic tumor-targeted gene transfer. Bioconjugate Chem 14, 222-231.

Lacoeuille, F., Hindré, F., Moal, F., Roux, J., Passirani, C., Couturier, O., Cales, P., Le Jeune, J.J., Lamprecht, A., Benoit, J.P., 2007. In vivo evaluation of lipid nanocapsules as a promising colloidal carrier for paclitaxel. Int J Pharm 344, 143-149.

Lamprecht, A., Saumet, J.-L., Roux, J., Benoit, J.-P., 2004. Lipid nanocarriers as drug delivery system for ibuprofen in pain treatment. Int J Pharm 278, 407-414.

Lee, H., Fonge, H., Hoang, B., Reilly, R.M., Allen, C., 2010. The effects of particle size and molecular targeting on the intratumoral and subcellular distribution of polymeric nanoparticles. Mol Pharm 7, 1195-1208.

Meng, H., Xue, M., Xia, T., Ji, Z., Tarn, D.Y., Zink, J.I., Nel, A.E., 2011. Use of size and a copolymer design feature to improve the biodistribution and the enhanced permeability and retention effect of doxorubicin-loaded mesoporous silica nanoparticles in a murine xenograft tumor model. ACS Nano 5, 4131-4144.

Mévellec, F., Tisato, F., Refosco, F., Roucoux, A., Noiret, N., Patin, H., Bandoli, G., 2002. Synthesis and characterization of the "sulfur-rich" bis (perthiobenzoato) (dithiobenzoato) technetium (III) heterocomplex. Inorg Chem 41, 598-601.

Morille, M., Montier, T., Legras, P., Carmoy, N., Brodin, P., Pitard, B., Benoit, J.-P., Passirani, C., 2010. Long-circulating DNA lipid nanocapsules as new vector for passive tumor targeting. Biomaterials 31, 321-329.

Morille, M., Passirani, C., Dufort, S., Bastiat, G., Pitard, B., Coll, J.-L., Benoit, J.-P., 2011. Tumor transfection after systemic injection of DNA lipid nanocapsules. Biomaterials 32, 2327-2333.

Müller, R.H., Shegokar, R., Keck, C.M., 2011. 20 years of lipid nanoparticles (SLN & NLC): present state of development & industrial applications. Curr Drug Discov Technol 8, 207-227.

Na, J.H., Koo, H., Lee, S., Min, K.H., Park, K., Yoo, H., Lee, S.H., Park, J.H., Kwon, I.C., Jeong, S.Y., Kim, K., 2011. Real-time and non-invasive optical imaging of tumor-targeting glycol chitosan nanoparticles in various tumor models. Biomaterials 32, 5252-5261.

Paillard, A., Hindré, F., Vignes-Colombeix, C., Benoit, J.-P., Garcion, E., 2010. The importance of endo-lysosomal escape with lipid nanocapsules for drug subcellular bioavailability. Biomaterials 31, 7542-7554.

Peltier, S., Oger, J.-M., Lagarce, F., Couet, W., Benoit, J.-P., 2006. Enhanced oral paclitaxel bioavailability after administration of paclitaxel-loaded lipid nanocapsules. Pharm Res 23, 1243-1250.

Perrault, S.D., Walkey, C., Jennings, T., Fischer, H.C., Chan, W.C.W., 2009. Mediating tumor targeting efficiency of nanoparticles through design. Nano Lett 9, 1909-1915.

Razkin, J., Josserand, V., Boturyn, D., Jin, Z.-h., Dumy, P., Favrot, M., Coll, J.-L., Texier, I., 2006. Activatable fluorescent probes for tumour-targeting imaging in live mice. ChemMedChem 1, 1069-1072.

Sancey, L., Dufort, S., Josserand, V., Keramidas, M., Righini, C., Rome, C., Faure, A.C., Foillard, S., Roux, S., Boturyn, D., Tillement, O., Koenig, A., Boutet, J., Rizo, P., Dumy, P., Coll, J.L., 2009. Drug development in oncology assisted by noninvasive optical imaging. Int J Pharm 379, 309-316.

Schädlich, A., Caysa, H., Mueller, T., Tenambergen, F., Rose, C., Göpferich, A., Kuntsche, J., Mäder, K., 2011a. Tumor accumulation of NIR fluorescent PEG-PLA nanoparticles: impact of particle size and human xenograft tumor model. ACS Nano 5, 8710-8720.

Schädlich, A., Hoffmann, S., Mueller, T., Caysa, H., Rose, C., Göpferich, A., Li, J., Kuntsche, J., Mäder, K., 2012. Accumulation of nanocarriers in the ovary: a neglected toxicity risk? J Control Release 160, 105-112.

Schädlich, A., Rose, C., Kuntsche, J., Caysa, H., Mueller, T., Göpferich, A., Mäder, K., 2011b. How stealthy are PEG-PLA nanoparticles? An NIR *in vivo* study combined with detailed size measurements. Pharm Res 28, 1995-2007.

Sonavane, G., Tomoda, K., Makino, K., 2008. Biodistribution of colloidal gold nanoparticles after intravenous administration: effect of particle size. Colloid Surf B 66, 274-280.

Sun, X., Rossin, R., Turner, J.L., Becker, M.L., Joralemon, M.J., Welch, M.J., Wooley, K.L., 2005. An assessment of the effects of shell cross-linked nanoparticle size, core composition, and surface PEGylation on *in vivo* biodistribution. Biomacromolecules 6, 2541-2554.

Torchilin, V., 2007. Micellar nanocarriers: Pharmaceutical perspectives. Pharm Res 24, 1-16.

Torchilin, V.P., 2005. Recent advances with liposomes as pharmaceutical carriers. Nat Rev Drug Discov 4, 145-160.

Vanpouille-Box, C., Lacoeuille, F., Belloche, C., Lepareur, N., Lemaire, L., LeJeune, J.-J., Benoit, J.-P., Menei, P., Couturier, O.F., Garcion, E., Hindré, F., 2011a. Tumor eradication in rat glioma and bypass of immunosuppressive barriers using internal radiation with 188Re-lipid nanocapsules. Biomaterials 32, 6781-6790.

Vanpouille-Box, C., Lacoeuille, F., Roux, J., Aubé, C., Garcion, E., Lepareur, N., Oberti, F., Bouchet, F., Noiret, N., Garin, E., Benoit, J.-P., Couturier, O., Hindré, F., 2011b. Lipid nanocapsules loaded with rhenium-188 reduce tumor progression in a rat hepatocellular carcinoma model. PLoS ONE 6, e16926.

Weyland, M., Manero, F., Paillard, A., Grée, D., Viault, G., Jarnet, D., Menei, P., Juin, P., Chourpa, I., Benoit, J.P., Grée, R., Garcion, E., 2011. Mitochondrial targeting by use of lipid nanocapsules loaded with SV30, an analogue of the small-molecule Bcl-2 inhibitor HA14-1. J Control Release 151, 74-82.

Vonarbourg, A., Passirani, C., Saulnier, P., Benoit, J.-P., 2006. Parameters influencing the stealthiness of colloidal drug delivery systems. Biomaterials 27, 4356-4373.

Vonarbourg, A., Saulnier, P., Passirani, C., Benoit, J.-P., 2005. Electrokinetic properties of noncharged lipid nanocapsules: Influence of the dipolar distribution at the interface. Electrophoresis 26, 2066-2075.

Yang, Z., Leon, J., Martin, M., Harder, J.W., Zhang, R., Liang, D., Lu, W., Tian, M., Gelovani, J.G., Qiao, A., Li, C., 2009. Pharmacokinetics and biodistribution of near-infrared fluorescence polymeric nanoparticles. Nanotechnol 20, 165101.

Yang, Z., Zheng, S., Harrison, W.J., Harder, J., Wen, X., Gelovani, J.G., Qiao, A., Li, C., 2007. Long-circulating near-infrared fluorescence core-cross-linked polymeric micelles: synthesis, characterization, and dual nuclear/optical imaging. Biomacromolecules 8, 3422-3428.

Zou, J., Saulnier, P., Perrier, T., Zhang, Y., Manninen, T., Toppila, E., Pyykkö, I., 2008. Distribution of lipid nanocapsules in different cochlear cell populations after round window membrane permeation. J Biomed Mat Res B 87B, 10-18.

Figure captions

Table 1. Compositions of LNC of different sizes.

	Solutol® (mg)	Lipoid® (mg)	Labrafac® (mg)	NaCl (mg)	Water (mg)	Concentration (mg/mL)
LNC 25 nm	645	25	282	30	685	168
LNC 50 nm	282	25	343	30	987	115
LNC 100 nm	161	25	403	30	1048	104

515

Table 2. Size and ζ-potential of ^{99m}Tc-LNC measured in physiological PBS.

	Diameter (nm)	PdI	ζ-Potential (mV)
LNC 25 nm	25±2	0.08	-3±1
LNC 50 nm	51±1	0.03	-4±1
LNC 100 nm	93±1	0.04	-6±1

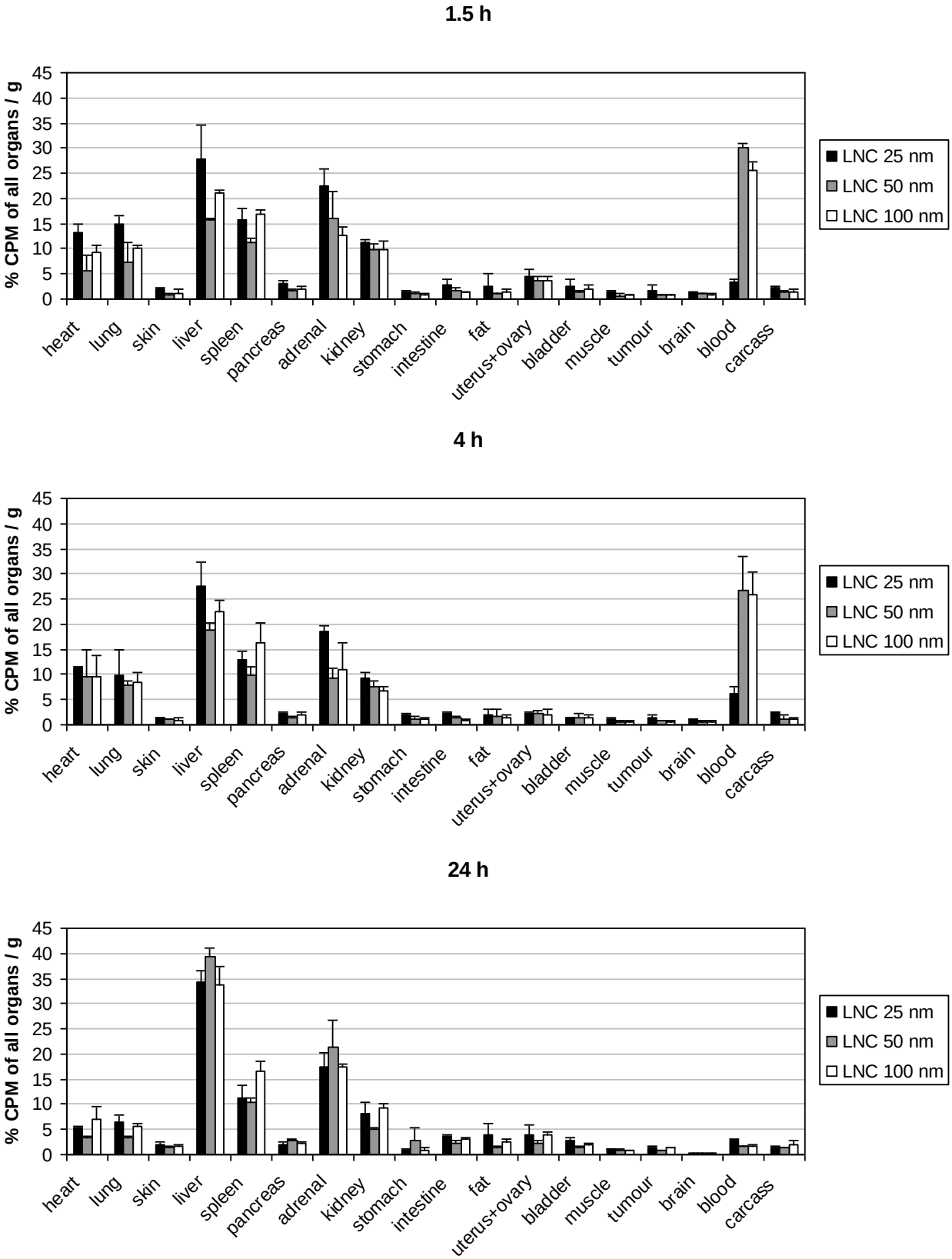

520 Figure 1. Biodistribution of 25, 50, and 100 nm ^{99m}Tc-LNC in different organs 1.5 h, 4 h, and 24 h after intravenous injection. CPM = counts per minute

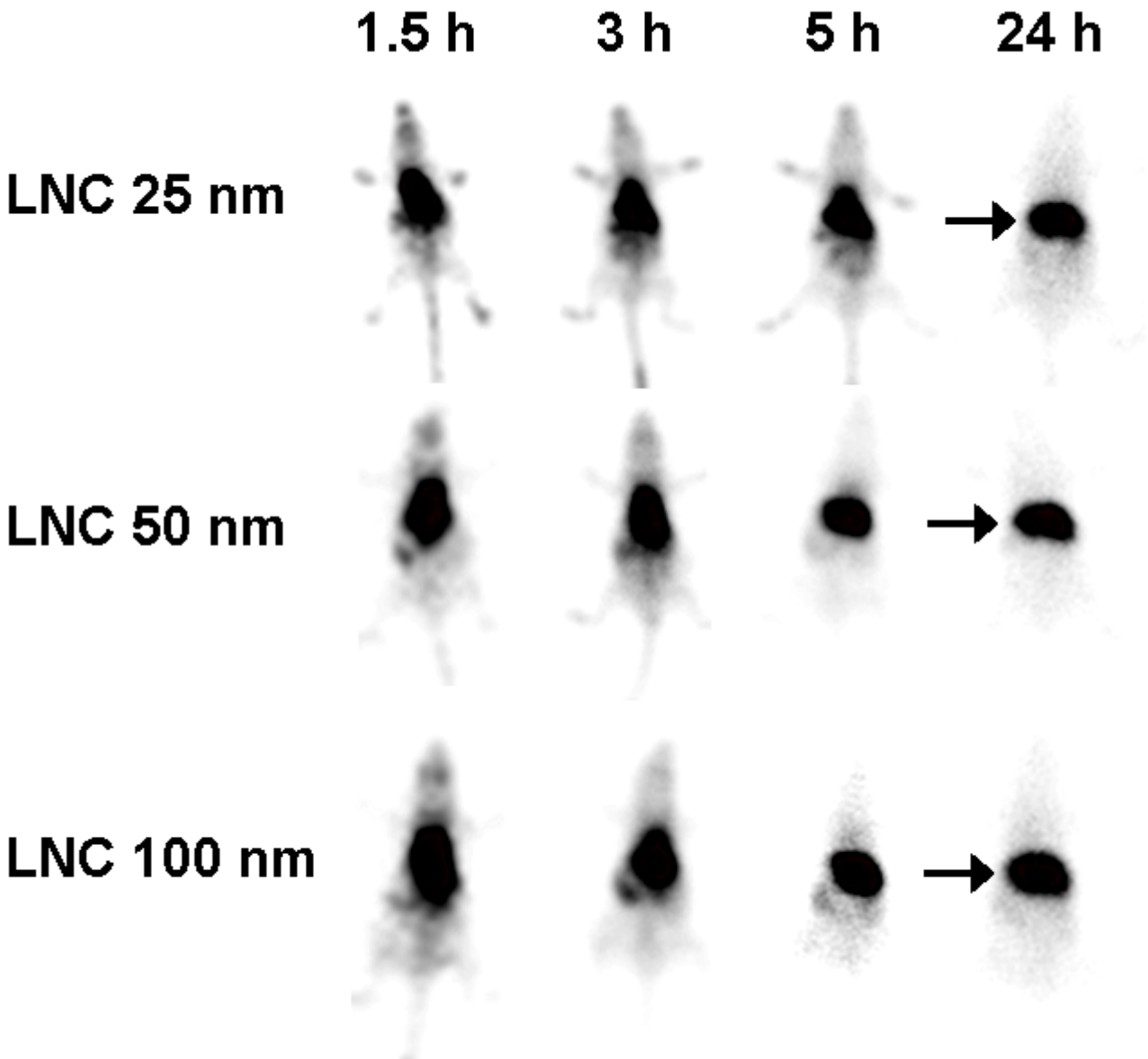

525 Figure 2. γ-Scintigraphic images expressing biodistribution of 25, 50, and 100 nm ^{99m}Tc-LNC in mice 1.5 h, 3 h, 5 h, and 24 h after intravenous injection. Arrows indicate the liver.

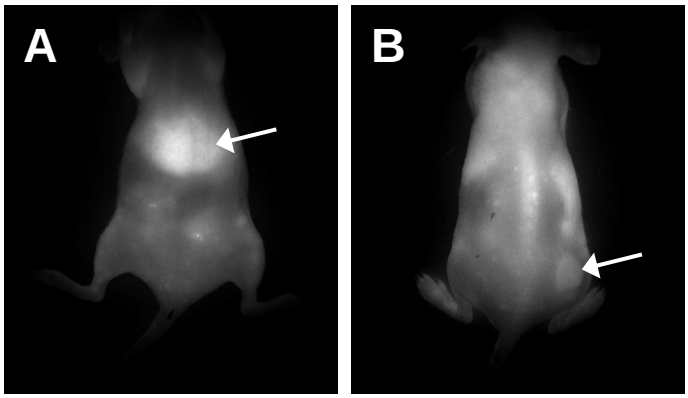

Figure 3. LNC biodistribution by optical imaging. Fluorescence images of a mouse 24 h after an i.v. injection of a 50%-50% mixture of 50 nm ^{99m}Tc-LNC and 50 nm DiD-LNC. Mouse lying on its back (A, arrow indicates the liver) and belly (B, arrow indicates the tumour).

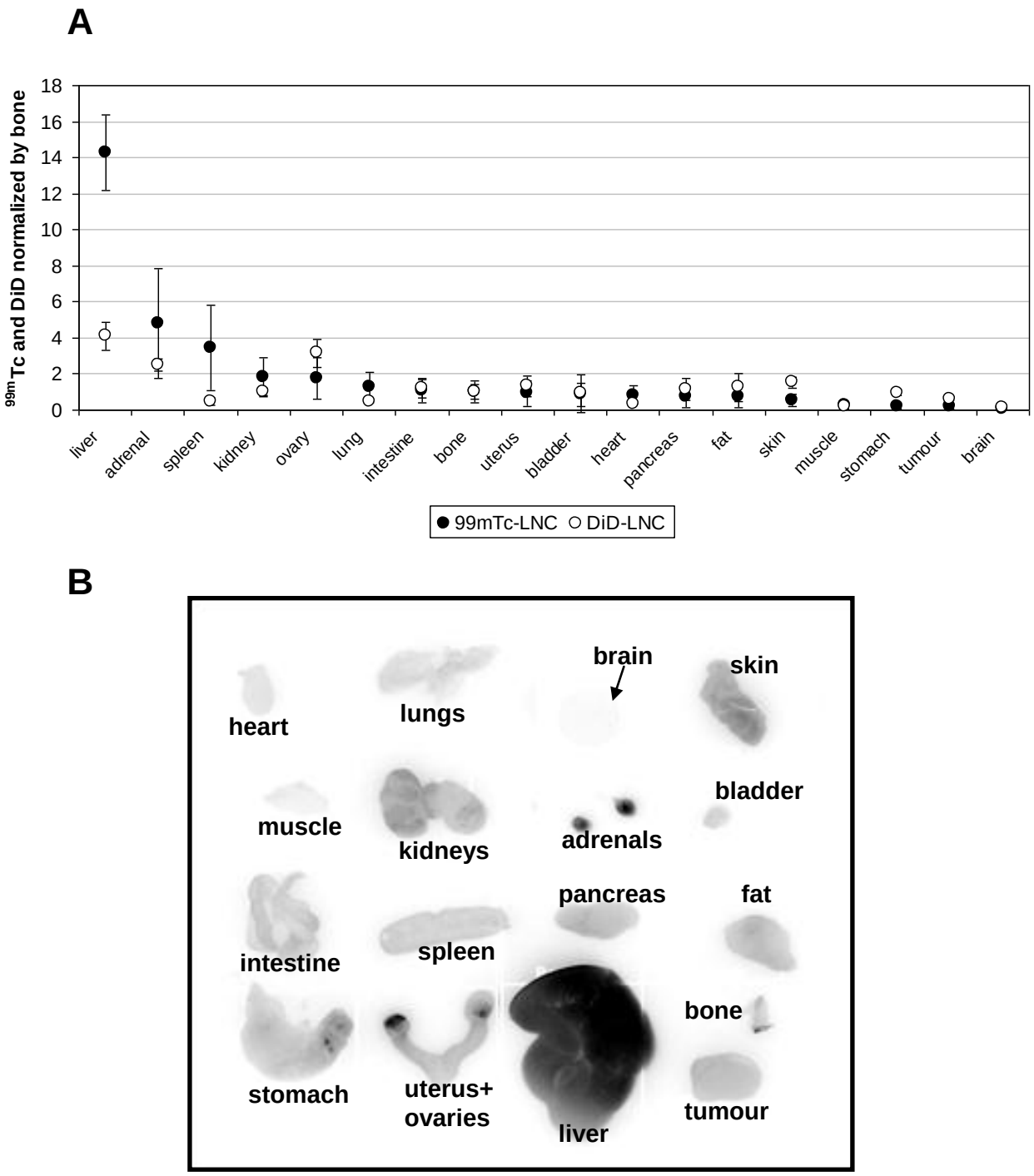

535

Figure 4. Comparison of the two detection techniques, radioactivity and fluorescence intensity, for quantification of organ distribution of the 50%-50% mixture (50 nm DiD-LNC and ^{99m}Tc-LNC) 24 h after injection (A). Example of the dissected organs visualized by a fluorescence camera (B).